Composite Structures 136 (2016) 16–24

Contents lists available at ScienceDirect

Composite Structures

journal homepage: www.elsevier.com/locate/compstruct

Simplified analytical model and balanced design approach for light-weight wood-based structural panel in bending

Jinghao Li [a,b], John F. Hunt [b,*], Shaoqin Gong [a], Zhiyong Cai [b,*]

[a] Department of Biomedical Engineering, Wisconsin Institutes for Discovery, and Materials Science and Engineering, University of Wisconsin-Madison, Madison, WI 53715, United States

[b] USDA Forest Service, Forest Products Laboratory, Madison, WI 53726, United States

ARTICLE INFO

Article history:
Available online 30 September 2015

Keywords:
Analytical modeling
Failure criterion
Mechanical testing
Balanced design
Bending behavior
Tri-axial core

ABSTRACT

This paper presents a simplified analytical model and balanced design approach for modeling light-weight wood-based structural panels in bending. Because many design parameters are required to input for the model of finite element analysis (FEA) during the preliminary design process and optimization, the equivalent method was developed to analyze the mechanical performance of panels based on experimental results. The bending deflection, normal strain and shear strain of the panels with various configurations were investigated using four point bending test. The results from the analytical model matched well with the experimental data, especially, the prediction for maximum deflection of the panels under failure load. The normal strain and shear strain calculated by the model also agreed with the experimental data. The failure criterion was determined by the failure modes using a 3-dimensional diagram with apparent normal and shear strain. For demonstration, panels 1 and 2 with a fixed core were modeled using the balanced design approach for optimal face thickness. The results showed that both the 3-dimensional diagram and analytical model provided similar thickness results, which were verified by the FEA for wood-based structural panels.

1. Introduction

Sandwich composites provide light-weight and high-strength characteristics that are widely used for many applications, ranging from aerospace and marine, to less demanding applications in transportation and building systems [1–4]. The sandwich structures of two thin skins with a structural core are generally produced using metal or fiber-reinforced-polymer (FRP) composites. The typical structural core can be formed using various structural cores (i.e.: honeycomb cores, foam cores, corrugated cores, truss cores, and grid cores), each of these have unique characteristics for specific applications. In 1964, the concept of an isogrid structural core made from aluminum was first proposed in the field of aerospace. The structural pattern of triangular trusses was shown to be very efficient [5]. Thus subsequent researchers continued to study isogrid structures to determine its mechanical characteristics, manufacturing methods, and applications [5–7]. In recent years, FRP materials have been widely used for many types of isogrid structures, which have demonstrated excellent performance characteristics. Fan et al. demonstrated improved compression and bending performance for lattice grid panels made from carbon fiber [8]. Several manufacturing methods have been proposed to construct the isogrid structures [9–11]. An isogrid fabrication process using carbon fiber and epoxy composite prepreg tow and unidirectional tape was introduced [12], and another manufacturing method used interlocked composite grid arrangement that could be used to simplify the assembly by using prefabricated materials [13]. For the aerospace and marine applications, the development and application of isogrid structures were summarized [14,15]. These studies used metal or FRPs for higher-value applications. There is no known literature for a core or structural panel that uses the isogrid made from renewable materials such as wood-based materials. There is a unique challenge and opportunity to extend the field of engineering applications using the isogrid core with green materials to develop new structural composites from light-weight engineered materials.

Forest Products Laboratory (FPL) has developed an eco-friendly tri-gird or tri-axial isogrid core structural panel made using phenolic impregnated laminated paper composites from our renewable forestry [16,17]. This research was initially sponsored by U.S. Department of Defense to look for alternative sustainable materials to substitute the current aluminum and other expensive alloy

* Corresponding authors. Tel.: +1 608 231 433; fax: +1 608 231 9582 (J.F. Hunt). Tel.: +1 608 231 9446; fax: +1 608 231 9582 (Z. Cai).

E-mail addresses: jfhunt@fs.fed.us (J.F. Hunt), zcai@fs.fed.us (Z. Cai).

http://dx.doi.org/10.1016/j.compstruct.2015.09.045
0263-8223/Published by Elsevier Ltd.

materials for its air transportation pallets and tactical shelters. As required, high strength, light weight, and water resistance were the top criterions in selecting the alternative products. Thus, this developed renewable structural panel also could be used for building construction, transportation, packaging, container with benefits to protect our environment. To produce the cost effective tri-axial isogrid core structural sandwich panels for difference applications, we need to develop a predicted model to simulate the overall performance of the panel with the configuration of each constitutive member to ensure a proper design. In the previous research [16,17], the simple I beam equation was applied to evaluate the bending properties of these structural panels, but it only considered linear ribs in one direction and didn't consider any cross-rib influences for the core and was less accurate in predicting actual performance. Finite element analysis (FEA) with higher accuracy could be used to analyze the panels' complex behavior such as stress concentration and buckling. However, the FEA process requires more time to build an exact model that includes the complex nature of the structure and its multiple parameters, especially, during the preliminary design process and optimization. Thus, a new integrated equivalent model for these composite grid structures with or without skins is being proposed. The model used equivalent stiffness based on coordinate matrix transformation to evaluate the grid mechanical properties [9]. Other researchers have also used the equivalent modeling method to calculate the equivalent modulus for the material properties. Fang's model considered repeatable triangle elements for transforming the structural mechanical performance [18]. It provided an efficient method to evaluate the performance for preliminary design, but it was only designed for the equilateral triangle element structure in Fig. 1. In our study, a simplified orthogonal model was developed that included the ribs' intersection angle as a parameter (Fig. 2(b)) and repeatable elements based on equivalent stiffness. These changes simplified the model by eliminating the coordinate transformation matrix as compared to Chen's model [9]. It also improved design flexibility to include non-equilateral triangles compared with Fang's equilateral model. This enhancement improved the design potential that allows for easier core parameter changes during the preliminary design process. Recently, higher order deformation plate theory and layerwise theory have been developed by Ferreira [19–22] to analyze sandwich structure plates. Both theories provided higher accuracy than classical plate theory and had better outcomes, particularly for shear analysis. Our goal is to simplify the analytical model for preliminary design while reducing complexity and computational effort. The simplified model with or without core shear effect was used to analyze and predict the bending behavior in this work.

This study analyzed the bending behavior and developed a failure criterion for the wood-based structural panels made from phenolic-impregnated laminated paper with or without carbon fiber fabric bonded to the surfaces. The panels were made having an isogrid core. Four types of wood-based structural panels were fabricated each having a different configuration, and three replicates were tested for each type of wood-based structural panels. The panels were tested using four point bending test to determine bending load and deflection. Eight normal strain gages and four shear strain gages were attached to the panels to measure the strains at critical locations. The test results were compared with the analytical model and FEA model and then a preliminary failure criterion for bending was determined using failure modes and strain distributions plotted on a 3-Dimensional diagram. The 3-D diagram was further proposed as a possible method for balanced design for a structural panel with a fixed isogrid core.

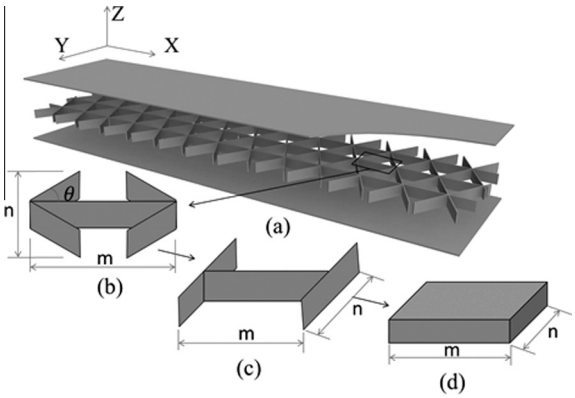

Fig. 2. Transformation process to achieve equivalent elemental properties for the tri-grid structural core: (a) structural panel configuration; (b) tri-grid element; (c) equivalent orthogonal element; (d) equivalent solid element.

2. Analytical modeling approach

2.1. The elemental transformation of tri-axial core structure

In our previous study, we transformed the tri-axial isogrid core into an equivalent solid core using repeatable element properties to achieve an equivalent stiffness approach. The tri-axial pattern of repeatable elements, Fig. 2(a), can be described as consisting of five ribs in different directions, Fig. 2(b). An equivalent rib section dimensions in the orthogonal directions were transformed based on angle θ under equivalent lengths, m and n, and core height, h_c shown in Fig. 2(a) or (b). The parameters of an equivalent solid core were obtained by transforming the elastic moduli, Poisson's ratios, and the shear moduli of rib material. The plane stress assumption was used in this model so that the relative properties along the 3-axis (Fig. 3) were ignored. The equivalent properties of E_X, E_Y, μ_{XY}, μ_{YX}, and G_{XY} for the tri-axial core can be obtained from the materials properties of E_1, E_2, μ_{12}, μ_{21} and G_{12} in the repeatable element through transforming the effective sections of the ribs to orthogonal equivalent sections, and then to an equivalent solid core. The progression of transformation is shown in Fig. 2(b)–(d).

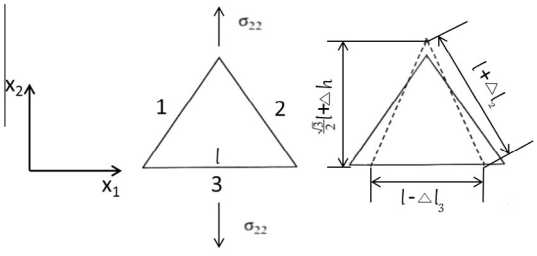

Fig. 1. The deformation of the equilateral triangular element for the isogrid structure.

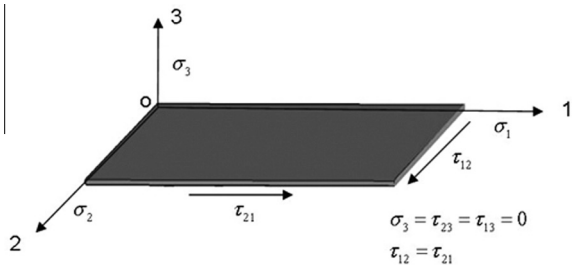

Fig. 3. Relative coordinate system for the plate materials.

The equivalent properties can be obtained from the transformation equations below [23–26]:

$$E_X = \frac{E_1 I_X}{I'_X} = \frac{E_1 a(1+cos\theta)}{n} \tag{1}$$

$$E_Y = \frac{E_1 I_Y}{I'_Y} = \frac{2E_1 a sin\theta}{m} \tag{2}$$

$$\mu_{XY} = \mu_{12} \tag{3}$$

$$\mu_{YX} = \frac{E_Y}{E_X}\mu_{XY} \tag{4}$$

$$G_{XY} = \frac{E_X E_Y}{E_X + E_Y + \mu_{YX}E_X + \mu_{XY}E_Y} \tag{5}$$

where θ is angle between the longitudinal rib and cross rib; a is rib thickness in the core; n is width for the equivalent solid element that perpendicular to X-axis; m is equivalent solid element width that perpendicular to Y-axis; E_1 is the elastic modulus in the machine direction for the relative coordinate system 1-axis for the laminated paper composites material (Fig. 3); E_X and E_Y are the elastic moduli on the X-axis and Y-axis of the equivalent solid element of the panel (Fig. 2); I_X, I_Y are the moment of inertias for orthogonal equivalent ribs on YZ-plane and XZ-plane; I'_X, I'_Y are the moment of inertia for solid plate element on the YZ-plane and XZ-plane; μ_{12}, is the Poisson's ratio for the rib material and μ_{XY}, and μ_{YX} are the Poisson's ratios for the equivalent solid plate element in both directions; and G_{XY} is the shear modulus of the equivalent solid plate element in the XY-plane.

The out-of-plane shear properties of the tri-axial structural core were analyzed under bending. For a structural panel with a large span-to-thickness ratio, shear deformation is small in the core and has little effect on core-skin bending deflection. However, core shear failure was one of the typical failure modes observed in the testing. It is important to determine the shear characteristic of the core. Based on the previous simplified orthogonal equivalent modeling, the out-of-plane shear modulus of the equivalent solid element in the span direction can be obtained from sectional transformation of the orthogonal equivalent element (Fig. 2(c)) based on the equivalent shear stiffness given by:

$$G_{XZ} = G_{ZX} = \frac{G_{12}A_X}{A'_X} = \frac{G_{12}a(1+cos\theta)}{n} \tag{6}$$

For core analysis in the orthogonal directions, the equivalent shear moduli can be given by:

$$G_{YZ} = G_{ZY} = \frac{G_{12}A_Y}{A'_Y} = \frac{2G_{12}asin\theta}{m} \tag{7}$$

where G_{12} is shear modulus of the rib; G_{XZ} and G_{YZ} are the shear moduli of the equivalent solid core in XZ-plane and YZ-plane; A_X and A_Y are sections of equivalent orthogonal element with respect to X-axis and Y-axis; A'_X and A'_Y are equivalent sections of solid element with respect to X-axis and Y-axis.

According to the geometric deformation, the shear strain relationship between the longitudinal rib and cross rib in the exact tri-axial structural core can be calculated based on trigonometric function:

$$\gamma_l = \frac{\gamma_c}{\cos\theta} \tag{8}$$

where γ_l is shear strain in the longitudinal rib, which is in 1–2 plane of rib material or XZ-plane of panel, and γ_c is shear strain in the cross rib in 1–2 plane of rib material.

If testing were in the Y-direction of the panel, the shear strain in the longitudinal rib becomes zero, and the shear strain in the Y-direction can be estimated within the cross ribs, which can be transformed by the equation:

$$\gamma_t = \frac{\gamma_c}{\sin\theta} \tag{9}$$

where γ_t is the transverse shear for the core orientation.

For bending test, the normal strain in the cross ribs between the loading points were ignored because the cross ribs were not continuous along the beam directions.

2.2. Laminated plate theory

According to the laminate plate theory, the wood-based structural panel composed of two skins sandwiched a structural core can be assumed to be three layers, thus the stress resultants N and stress couples M in Fig. 4 are given by:

$$\begin{Bmatrix} N_X \\ N_Y \\ N_{XY} \end{Bmatrix} = W\sum_{k=1}^{3}\left(\int_{h_{k-1}}^{h_k}[Q]_k \begin{Bmatrix} \varepsilon_{X_0} \\ \varepsilon_{Y_0} \\ \varepsilon_{X_0Y_0} \end{Bmatrix} dz + \int_{h_{k-1}}^{h_k}[Q]_k \begin{Bmatrix} \kappa_X \\ \kappa_Y \\ \kappa_{XY} \end{Bmatrix} zdz\right) \tag{10}$$

$$\begin{Bmatrix} M_X \\ M_Y \\ M_{XY} \end{Bmatrix} = W\sum_{k=1}^{3}\left(\int_{h_{k-1}}^{h_k}[Q]_k \begin{Bmatrix} \varepsilon_{X_0} \\ \varepsilon_{Y_0} \\ \varepsilon_{X_0Y_0} \end{Bmatrix} zdz + \int_{h_{k-1}}^{h_k}[Q]_k \begin{Bmatrix} \kappa_X \\ \kappa_Y \\ \kappa_{XY} \end{Bmatrix} z^2dz\right) \tag{11}$$

where W is width of panel; N_X and N_Y are normal force in X-axis and Y-axis; N_{XY} is in-plane shear stress in XY-plane; M_X, M_Y and M_{XY} are moments with respect to N_X, N_Y and N_{XY}; k is the layer number of the sandwich panel; h is thickness of each layer. ε_{X_0} and ε_{Y_0} are strain respect to the neutral axis of X and Y directions; $\varepsilon_{X_0Y_0}$ is shear strain in XY-plane; κ_X and κ_Y are curvature in X-axis and Y-axis; κ_{XY} is the curvature respect to XY combination; z is location of plate boundary; and $[Q]_k$ is the stiffness matrix for the particular layer. The stiffness matrix of skin and core are given by:

$$[Q]_s = \begin{bmatrix} \frac{E_1}{1-\mu_{12}\mu_{21}} & \frac{\mu_{21}E_2}{1-\mu_{12}\mu_{21}} & 0 \\ \frac{\mu_{12}E_1}{1-\mu_{12}\mu_{21}} & \frac{E_2}{1-\mu_{12}\mu_{21}} & 0 \\ 0 & 0 & G_{12} \end{bmatrix} \tag{12}$$

$$[Q]_c = \begin{bmatrix} \frac{E_X}{1-\mu_{XY}\mu_{YX}} & \frac{\mu_{YX}E_Y}{1-\mu_{XY}\mu_{YX}} & 0 \\ \frac{\mu_{XY}E_X}{1-\mu_{XY}\mu_{YX}} & \frac{E_Y}{1-\mu_{XY}\mu_{YX}} & 0 \\ 0 & 0 & G_{XY} \end{bmatrix} \tag{13}$$

where $[Q]_s$ is stiffness matrix of skin and $[Q]_c$ is stiffness matrix of core.

We assumed that out-of-plane shear force in the two skins had no noticeable effect on the bending deflection because the core thickness was more than 6 times thicker than the skin thickness. Therefore, the shear force in the skins can be ignored in the calculation. The shear force was supported primarily by the structural core during bending, so the out-of-plane shear force of the equivalent solid core can be expressed as:

$$\begin{Bmatrix} Q_{XZ} \\ Q_{YZ} \end{Bmatrix} = W\int_{-\frac{h_c}{2}}^{\frac{h_c}{2}} \begin{bmatrix} G_{XZ} & 0 \\ 0 & G_{YZ} \end{bmatrix} \begin{Bmatrix} \gamma_{XZ} \\ \gamma_{YZ} \end{Bmatrix} dz \tag{14}$$

where h_c is the height of the core; Q_{XZ}, γ_{XZ}, and Q_{YZ}, γ_{YZ} are shear forces and shear strains in the XZ-plane and YZ-plane, respectively.

Based on the equivalent transformed Eqs. (6) and (7) combined with shear force Eq. (14), the shear forces in the equivalent solid

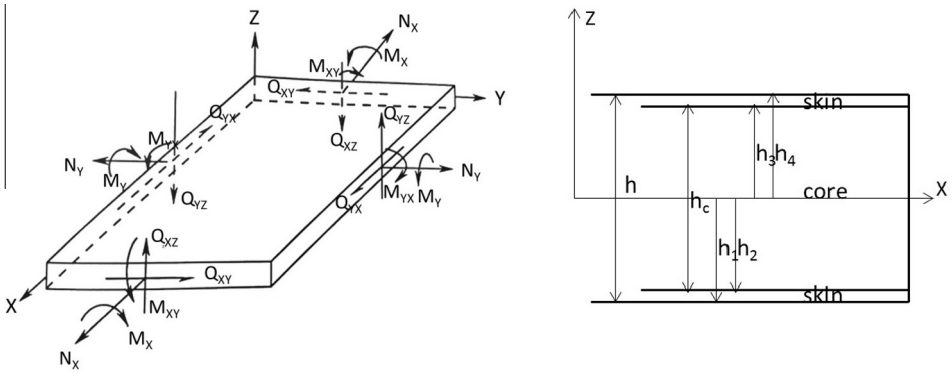

Fig. 4. The stress resultants and stress couples for a plate.

core also can be calculated by the shear modulus of ribs in the core, Eq. (15):

$$\begin{Bmatrix} Q_{XZ} \\ Q_{YZ} \end{Bmatrix} = W \int_{-\frac{h_c}{2}}^{\frac{h_c}{2}} \begin{bmatrix} \frac{a(1+\cos\theta)}{n} & 0 \\ 0 & \frac{2a\sin\theta}{m} \end{bmatrix} \begin{bmatrix} G_{12} & 0 \\ 0 & G_{12} \end{bmatrix} \begin{Bmatrix} \gamma_{XZ} \\ \gamma_{YZ} \end{Bmatrix} dz \tag{15}$$

In this analytical model, both normal and shear forces can be calculated using the corresponding strains and material properties according to the load and boundary conditions. Similarly, the inverse matrices (10), (11), (14) and (15) can be used to calculate the strain and bending characteristics based on bending load.

2.3. Reduced beam formulas based on plate theory for four point bending

Based on laminated plate theory, the relationship between the bending moment and geometry for bending analysis of a symmetric beam can be given by:

$$\{M\} = [D]\{\kappa\} \tag{16}$$

or

$$\{\kappa\} = [D^*]\{M\} \tag{17}$$

where the matrix $[D^*]$ is the inverse of the bending–twisting stiffness matrix $[D]$.

For a simply supported beam, the assumption was given by:

$$M_X = M_Z = 0 \tag{18}$$

Then the bending strain of our panel in the mid-span section under third point loading configuration can be given by:

$$\varepsilon = t\kappa_X = \frac{dPR}{2W} D^* \tag{19}$$

where d is the distance from the neutral axis to strain position on the beam transverse section; P is the total bending load; Relative D^* is obtained from matrix $[D^*]$; R is the distance from the load point to the neighboring support; and W is the width of the panel.

The maximum shear strain in the rib of the core can be calculated by the shear stress and shear modulus. The shear stress can be obtained by Eq. (20):

$$\tau = \frac{VJ}{I_z W} \tag{20}$$

where V is total shear force, which equals $1/2P$ of total load for bending; J is the static moment; and I_z is moment of inertia of the entire cross sectional area. The sandwich panel can be considered as a composite beam to evaluate the bending behavior and then the core with different mechanical properties, apart from the skins, can be simplified using the equivalent I-beam approach.

Therefore, the shear strain in the core can be written by Eq. (21):

$$\gamma = \propto \frac{\tau}{G_{12}} = \propto \frac{PJ}{2I_z W G_{12}} \tag{21}$$

where $\propto$ is shear coefficient that depends on the geometry and $\propto$ was assumed 1 for this analysis.

The bending displacement equation without considering shear effects can be given by Eq. (22):

$$\omega_{z,b} = \frac{D^* P}{96W}(6RL^2 - 8R^3) \tag{22}$$

where $\omega_{z,b}$ is displacement in the Z-direction; L is the beam span. The bending deflection combined with shear deflection in the core for total deflection of our panel was compared with the result of Eq. (22), thus the mid-span deflection for bending of the panel could be calculated including bending displacement of the panel plus vertical displacement due to core shear strain.

The shear contribution to bending deflection for third point loading configuration can be calculated by Eq. (23) in terms of geometrical relationship:

$$\omega_{z,s} = \frac{\tau L}{3G_{12}} = \propto \frac{PLJ}{6I_z W G_{12}} \tag{23}$$

The total mid-span defection is given by:

$$\omega_{z,t} = \frac{D^* P}{96W}(6RL^2 - 8R^3) + \propto \frac{PLJ}{6I_z W G_{12}} \tag{24}$$

where $\omega_{z,t}$ is mid-span displacement; relative D^* is obtained from $[D^*]$.

3. Materials properties

The mechanical properties used for this study were obtained by testing according to ASTM test methods D638 and D695 (ASTM 2010; ASTM 2010) [29,30]. Phenolic impregnated laminated paper 2.36 mm thick with a density of 1387 kg/m^3, NP610 (Norplex-Micarta Inc., Postville, IA) was used for the core and skins. Carbon fiber fabric, a tri-axial woven material, QISO, A&P Technology, (San Jose, California, USA) was bonded to both outside skins of panels using U.S. Composites (West Palm Beach, Florida, USA) epoxy resin no. 635 [16].The materials properties were shown in Table 1.

The epoxy resin no. 635 (US Composites Inc.) was formed into a dog-bone test coupon and tensile tested. The epoxy resin was assumed to be isotropic. The shear modulus of epoxy resin was estimated by the formula for isotropic materials:

$$G = \frac{E}{2(1+\mu)} \tag{25}$$

Table 1
Materials properties of structural panels.

Materials	Nominal thickness (mm)	Comp. strength MD[b] (MPa)	Comp. strength CD[c] (MPa)	Tensile strength MD[b] (MPa)	Tensile strength CD[c] (MPa)	MOE MD[b] (GPa)	MOE CD[c] (GPa)	Shear modulus (GPa)	Poisson ratio MD	Poisson ratio CD
Laminated papers (LP)	2.36	195.1	168.7	173.9	118.6	11.6	8.3	4.3	0.36	0.27
Carbon fiber fabric/L[a]	3.15	195.1	168.7	216.6	132.2	16.3	13.6	6.0	0.36	0.46
Epoxy resin	–	105.9	–	31.0	–	1.4	–	0.54	0.3	–

Note:
[a] Carbon fiber fabric bonded with laminated paper composite.
[b] MD is an abbreviation of machine direction (1-axis).
[c] CD is an abbreviation of cross direction (2-axis).

The epoxy resin strength was determined according lap shear test method ASTM D5868 [16,32], the average epoxy shear strength was 17.9 MPa between the laminated paper.

4. The experimental design for bending test

Four types of experimental panels were made were fabricated for testing. The panels were fabricated with tri-axial core configuration using laminated paper ribs. The nominal height of rib was 33.0 mm. The slots in the core pieces were cut slightly oversized to account for the 60° angular orientation between the ribs when assembled. The distance between slots for all pieces was 117.3 mm, thus creating an equilateral triangle with a core density of 65 kg/m^3. Three main ribs were aligned with either the MD or CD of skins for different panels, see Fig. 2. The panels were fabricated so that the ribs were centrally positioned and width determined to include three complete longitudinal ribs. Panel 1 was made with 1 layer laminated paper skins and MD core only; panel 2 was made with two layers of laminated paper skins and MD fiber direction core, panel 3 was made with two layers laminated paper skins and CD fiber direction core; and panel 4 was made with laminated paper composited carbon fiber fabric skins with MD fiber direction core, see Table 2. When additional carbon fiber fabric or laminated paper sheet were added the surfaces were sanded before epoxy was applied. The primary alignment for the carbon-fiber fabric or additional laminated paper sheet aligned with the MD of the skins. The fabrication process of tri-axial structural panel is shown in Fig. 5.

The four point bending test for third point loading configuration, ASTM C393 (ASTM 2006) [31], was used to test the panels. To verify the strain distributions in the panels during the bending test, strain gages were placed inside one panel from each configuration. Twelve strain gages including 8 normal strain gages (CEA-06-250UN-350) and 4 shear strain gages (CEA-06-187UV-350) (Micro-Measurements Inc) were bonded to the surface of the ribs or faces for measuring the strain of the critical locations on the panels [27]. The strain gage locations are shown in Fig. 6. Five LVDTs were placed beneath the panels at 1/6, 1/3, 1/2, 2/3 and 5/6 the span to measure bending deflection. The test set-up dimension and testing device positions are shown in Fig. 7. This was our first attempt to investigate both shear and tension strain distributions within the sandwich construction panel. There were a considerable complexity and high cost of applying strain gages within the panels. Since all the panels were fabricated from impregnated laminated paper composite material which was very uniform and consistent in their mechanical performance with less than 5% in coefficient of variance [27]. After consulting with a statistician, we constructed one panel for each configuration and believed that the strain distribution results were representative for the other panels tested with the same configuration.

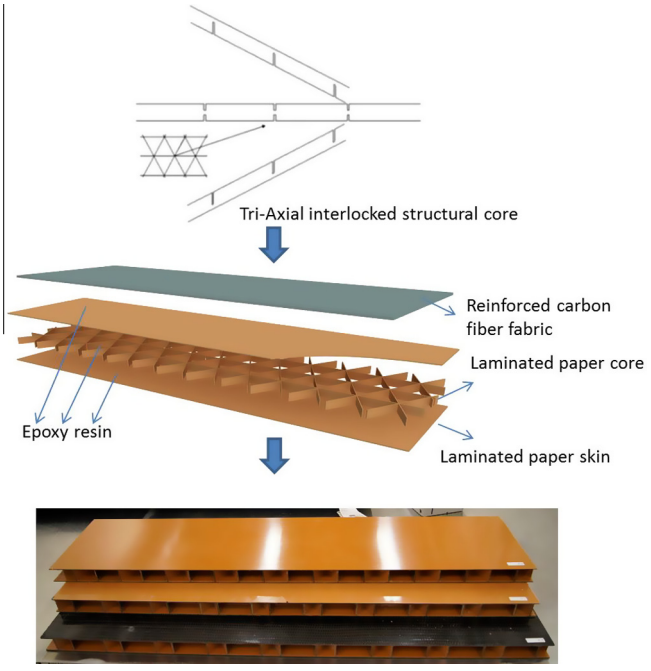

Fig. 5. Tri-axial structural panel fabrication from linear ribs that are either double slotted or single slotted.

5. Results and discussions

5.1. Bending comparisons of experimental and modeling results

Table 3 shows the experimental, finite element analysis (FEA) and analytical modeling results for the four bending test panels. The top row within each group shows the results for the single panel test with strain gages. The second row within each group

Table 2
The bending panel dimensions and configurations.

ID (no.)	Skin materials	Core mechanical direction	Panel dimensions (mm)	Core height (mm)	Face thickness (mm)
1	One layer laminated paper	MD	914 × 267 × 37.6	32.5	2.6
2	Two layers laminated paper	MD	914 × 267 × 43.3	32.5	5.4
3	Two layers laminated paper	CD	914 × 267 × 42.9	32.5	5.1
4	Laminated paper composited carbon fiber fabric	MD	914 × 267 × 39.9	33.0	3.4

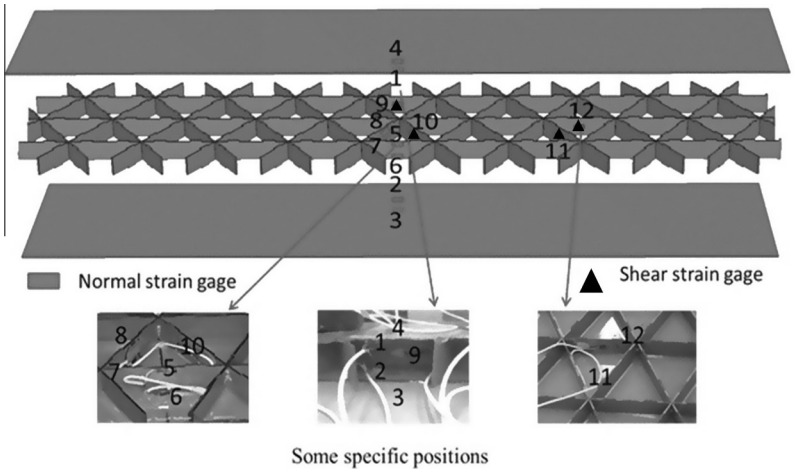

Fig. 6. Strain gage positions.

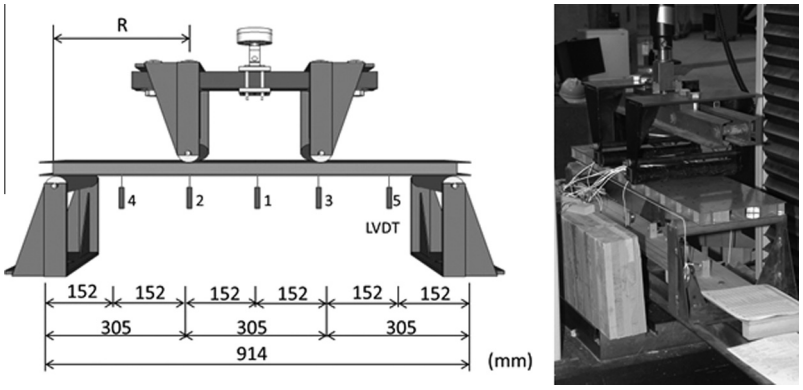

Fig. 7. Test dimensions, lvdt locations, and set-up for four point bending test.

Table 3
Strain and deflection of each experimental sandwich panel under failure load.

Panel ID (no.)	Failure load (kN)	Failure mode	Maximum normal strain ε on the skin ($\mu\varepsilon$)			Maximum shear strain γ in the core ($\mu\varepsilon$)			Maximum deflection (mm)			
			Exp.	FEA	Analyt.	Exp.	FEA	Analyt.	Exp.	FEA	Analyt. without shear effect	Analyt. with shear effect
1	11.6	Skin comp.	5028 (T)	5765 (T)	6251	2321	2635	1880	29.6	29.9	29.4	30.1
Avg.	11.7 (12.5)[a]		−7520 (C)	−7853 (C)					29.1 (2.8)			
2	18.4	Core shear	4011 (T)	4950 (T)	4849	4701	4859	4115	20.4	21.5	18.4	21.1
Avg.	19.4 (7.2)		−4351 (C)	5290 (C)					23.4 (9.6)			
3	21.8	Core shear	5160 (T)	5135 (T)	5833	5011	5009	4892	25.8	26.3	24.0	25.4
Avg.	21.2 (2.7)		−5524 (C)	−5507 (C)					25.1 (2.7)			
4	18.7	Core shear	5224 (T)	5696 (T)	5914	4827	4741	4525	29.3	28.2	26.9	28.2
Avg.	19.2 (3.9)		−5290 (C)	−5891 (C)					27.9 (4.7)			

Note:
[a] Number in parentheses is coefficients of variation, in percent. (T) is tensile strain. (C) is compressive strain.

shows the average results for all panels including the results from the panel with strain gages. For all the panels, the maximum normal strain was on the compression side which was larger than the tensile strain. We believe this occurred because localized compression buckling caused the additional strain. Panel 1 had the thinnest skins (Table 2), thus compression/buckling in the face occurred before the core shear failure occurred. In contrast, panels 2–4 had either twice the skin thickness (panels 2 and 3) or a layer of carbon fabric (panel 4). These thicker and stiffer skins were less susceptible to buckling and forced the failure to the core rather than failing in the skins. The stiffness ratio of faces-to-core significantly affected the location of the failure so that failure occurred on the lower stiffness component. Failure due to face compression buckling on the thin skinned panel (Panel 1) and core shear failure on the stiffer skinned panels (Panels 2–4) was as expected, Fig. 8 (a) and (b).

The critical shear strain at failure in the core (Table 3) was measured from the strain gage located at the neutral axis of the rib. The measured maximum shear core strain in our panel was slightly higher than what the model predicted. This was expected because

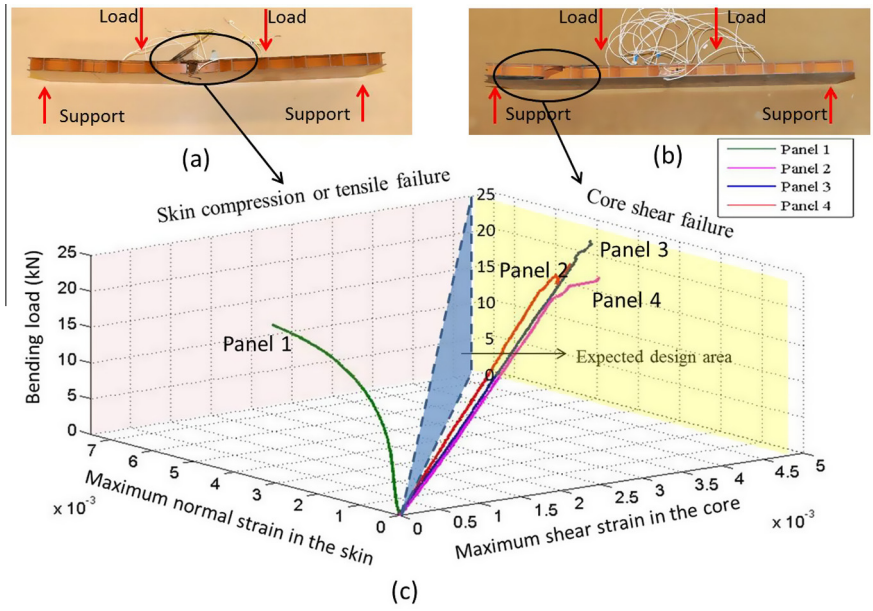

Fig. 8. Three-dimension diagram for failure modes and criterion.

the actual shear across the rib was distributed nonlinearly [28]. However, the analytical model with linear assumption predicted strain slightly less than experimental results, because it used a constant shear coefficient factor $\propto = 1$. The top skin compression buckling also had a small effect on the core that could have increased the measured shear strain on the rib. Thus the shear strain from the analytical model, while less than the experimental strain, was reasonable and acceptable estimate for preliminary design purposes. The results of FEA with each exact model of four types of panels had slightly higher accuracy than analytical model, but it required more time and computational effort to simulate the bending performance.

Deflections with and without core shear were evaluated. The analytical model with shear effect or without it fit within 10% error of the experimental data. The model predicted deflections for all panels with core shear effect that compared well with the experimental data. The average difference was approximately 2.5% and maximum difference was 3.5%. Without core shear effects, the model predicted deflections that had a higher error than when core shear effects were included. This indicates that shear strain deformation, while relatively small, still contributes to provide a better model prediction. The three panels with thicker skins configurations core shear failure were expected. The reason was that compared with core stiffness, the skin stiffness was significant larger in bending, thus the causing the core components to fail at the material's yield strength, while the strength of the skin components were still below its ultimate strength. We estimate that damage first occurred in the core-face interface and then propagated quickly to ribs causing core failure. The epoxy resin's mechanical properties are significantly lower than the laminated paper's properties and failure may have initiated at the interface.

5.2. Three-dimension analysis diagram

Fig. 8 represents the relationship of maximum normal strain on the skins, maximum shear strain on the ribs of core, and bending load. It displays the optimization of the failure modes for each sandwich panel. The normal skin strain is plotted on the *X*-axis, the shear strain in the core is plotted in the *Y*-axis, and the bending load is plotted on the *Z*-axis. As shown, panel 1 failed in compression on the top skin and panels 2–4 had core shear failures on the longitudinal ribs. The strain results for each panel accurately described the type of failure based on the material properties of the material. In Fig. 8, the end point for panel 1 failed when the normal strain was around 7520 με and is the pink surface indicating either skin compression or tensile failure. The end-points for the curves for panels 2–4 occurred at a shear strain around 4701 με and is indicated by the yellow shear area.

From the curve for panel 1, it demonstrated that the skins were insufficiently constructed for that core configuration. The shear strains on the rib of core for panel 1 were only around 2321 με while the normal strain on the skin reaches its maximum of 7520 με, where failure occurred. Whereas panel 2 had twice the skin layers thickness with the same core dimensions as panel 1, the plot for panel 2 shows the core did not have sufficient shear strength thus resulting in core shear failure. Shear strain had reached 4701 με while the maximum normal strain on the skins is only approximately 57.8% of the maximum of 7520 με. For panel 3, the core rib orientation had the paper laminate MD orientation turned 90° or perpendicular to the panel direction. This rotation provides higher shear strength because of the fiber orientation that provides better shear resistance within the ribs. The result of this rotation was an increase in the bending load for panel 3 that was higher than that of the other panels. With the two skin layers, the normal strain still did not reach the maximum failure strain before the panel failed. Panel 4 had even stiffer skins with thin carbon fiber fabric bonded to the surfaces of the panel. The result shows the maximum shear strain on the ribs was around 4827 με while the maximum normal strain on the skins was only around 5290 με at failure.

Usually sandwich panels are dominated by either failures of compression or tensile failure on skins or shear failure on the core. The failure criterion can be determined using the maximum normal strain on the skins and maximum shear strain on the ribs. In Fig. 8, the blue triangle represents the simultaneous failure of the skins and the core when making full use of the material's strength properties under bending. To achieve the light-weight and high-performance characteristics, the balanced parameters for configurations for wood-based structural panel need to be analyzed to achieve a balanced design.

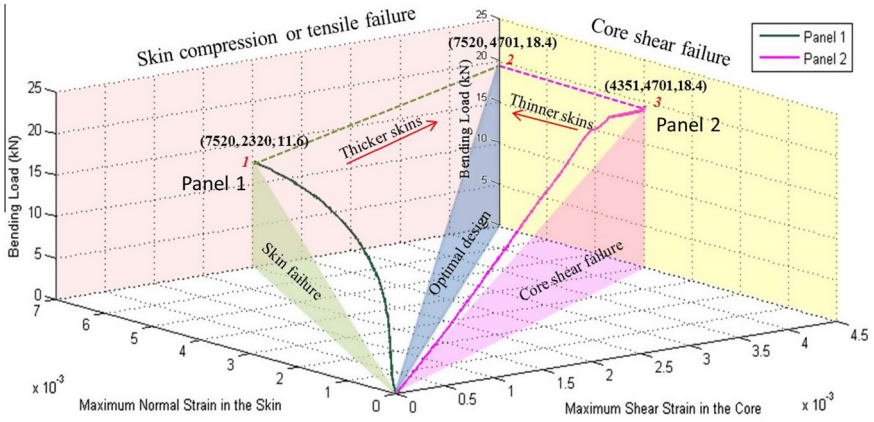

Fig. 9. Optimal three-dimension design map based on panel 1 and panel 2.

Table 4
Comparison between actual and optimal thickness of skins, normal strain, and shear strain for the actual structural panels and calculated by ANSYS, diagram analysis, and analytical modeling.

Panel ID	Skin thickness (mm)	Bending load (kN)	Failure normal strain on the skin (με)	Failure shear strain on the rib of core (με)
Panel 1	2.5	11.6	7520	2320
Panel 2	5.4	18.4	4351	4701
ANSYS optimization	4.31	18.4	7378	4894
Diagram analysis	4.47	18.4	7520	4501
Analytical modeling	3.57	18.4	7444	4511

5.3. Balanced design analysis

The initial panel configuration and analysis stages are important for a balanced design of any structural panel. An approximate method to help achieve this balanced design was developed based on optimization of the face normal strain and core shear strain. Fig. 9 shows the normal vs core shear strain test plots as a function of bending load for panels 1 and 2. The only difference between the two panels was that panel 1 had a single skin layer while panel 2 had a double thickness skin layer, Table 2. A "balanced" failure area was developed based on the area described by Eq. (27).

$$\Delta = \frac{\sqrt{(\epsilon^2 + \gamma^2)} \times P}{2} \tag{26}$$

where Δ is the failure area calculated from strain and bending load; ϵ is the apparent maximum normal strain on the skins; γ is the apparent maximum shear strain in the ribs; and P is the bending load. In Fig. 9, the estimated failure triangle area was determined from the results for panels 1 and 2. At point 1 (Panel 1), it illustrates that the skin thickness was too thin and failure would occur at the apparent maximum normal strain failure in the skins. At Point 1, the core shear for panel 1 was low and the core shear strain was not sufficient to cause failure. If the skin layer was doubled, point 3 (Panel 2), then the bending load could be increased to cause failure to shift to core shear. Having too thin or too thick of skins is still not balanced for the current panel core design. If the skin thickness were increased slightly from point 1 then the bending load increases as the skin apparent maximum normal strain was maintained. The effect on core shear strain was that it increased to maximum point 2 of the balanced design. If the skin thickness continued to increase, the load stayed the same but core shear would be the dominant failure criteria as shown by point 3. This process is useful to find the excepted or balanced design by determining simultaneously the skin normal strain and core shear strain failure. The balanced design case for panels 1 and 2 assumed the material properties were elastic and the relationship between the thickness of skin and failure triangle area had linear behavior for simplification. The apparent failure normal strain on both skins was assumed to be 7520 με and the failure apparent shear strain on the ribs was assumed to be 4701 με. Therefore, the balanced thickness of the skin using linear interpolation can be initially evaluated using Eq. (27) based from Fig. 9:

$$T_{\text{balanced}} = T_{\text{Panel1}}\left\{1 + (T_{\text{Panel1}} - T_{\text{Panel2}})\left[\frac{(\Delta_{\text{ob}} - \Delta_{\text{sf}})}{(\Delta_{\text{ob}} - \Delta_{\text{sf}}) + (\Delta_{\text{ob}} - \Delta_{\text{cf}})}\right]\right\} \tag{27}$$

where T_{Panel1} was the thickness of skins of panel 1, T_{Panel2} was the thickness of skins of panel 2, Δ_{ob} is the balanced failure triangle area, Δ_{sf} is the skin failure triangle area of panel 1, Δ_{cf} is the core failure triangle area of panel 2. For this study, the balanced thickness for the skins was determined using FEA and compared with the diagram analysis and the analytical model. All these models used the apparent failure normal strain for the skin and apparent failure shear strain for the rib, Table 4. The diagram analysis and FEA analysis provided similar results for the optimum skin thickness. The skin thickness calculated using analytical model was approximately 20% less than the diagram analysis and FEA analysis. The skin thickness was less because the analytical model used linear material property assumption that provides stiffer results. Even though the analytical model predicted a thinner balanced skin thickness it was still thicker than the skin thickness for panel 1. This result would have been acceptable for a first approximation and useful for preliminary design purposes.

6. Conclusions

The bending behavior of the wood-based structural panel can be evaluated and predicted using the analytical model. The prediction of the bending deflection by the model with core shear effects

had better accuracy than the model without core shear effects, especially on the core shear failure panels. The apparent normal strain for the skin and apparent shear strain for the rib were also analyzed using the analytical model approach. The model results fit well with the experimental results. Core shear strength affected the bending performance and failure mode. The failure criterion was defined using either the apparent maximum normal strain on the skins or the apparent maximum shear strain on the ribs to determine the failure load for the structural panels.

The 3-D diagram approach with axes of normal strain, shear strain and bending load was creatively produced to show the typical failure map based on the experimental results. The balanced design of the analytical model, 3-D diagram statistical analyses and FEA model were discussed based on panels 1 and 2 to predict the balanced thickness skins for the panel with the specific core. The skin thickness obtained using the diagram analysis and the analytical model were within +4% and −17% error which was checked using the FEA model, respectively. These balanced methods can be used to maximize the full use of all components in the structural panel for bending.

Acknowledgements

This work is supported by USDA, Forest Products Laboratory and the authors gratefully acknowledge the support of Sara Fishwild, James Bridwell, Marshall Begel, Dave Simpson and Marc Joyal of EMRSL group for the mechanical testing.

References

[1] Vasiliev VV, Barynin VA, Rasin AF. Anisogrid lattice structures survey of development and application. Compos Struct 2001;54:361–70.
[2] Wei X, Tran P, De Vaucorbeil A, Ramaswamy RB, Latourte F, Espinosa HD. Three-dimensional numerical modeling of composite panels subjected to underwater blast. J Mech Phys Solids 2013;61(6):1319–36.
[3] Davalos JF, Qiao PZ, Xu XF, Robinson J, Barth KE. Modeling and characterization of fiber-reinforced plastic honeycomb sandwich panels for highway bridge applications. Compos Struct 2001;52:441–52.
[4] Sharaf T, Fam A. Experimental investigation of large scale cladding sandwich panels under out-of-plane transverse loading for building applications. J Compos Constr 2011;13(3):422–30.
[5] Isogrid design handbook, NASA CR-124075, Isogrid design handbook, McDonnell Douglas Astronautics Company. 1973.2.
[6] Key JE. Isogrid structural tests and stability analyses. J Aircr 1976;13(10):778–85.
[7] Jenkins WC. Determination of critical buckling loads for isogrid-stiffened cylinders. McDonnell Douglas Report No. MDC-G2792. 1972.
[8] Fan HL, Meng FH, Yang W. Sandwich panels with Kagome lattice cores reinforced by carbon fibers. Compos Struct 2007;81(4):533–9.
[9] Chen HJ, Tsai SW. Analysis and optimum design of composite grid structures. J Compos Mater 1996;30(4):503–34.
[10] Tsai SW, Liu KS, Manne PM. Manufacture and design of composite grids. Mater Constr 1997;47:59–71.
[11] Huybrechts SM, Meink TE, Wegner PM, et al. Manufacturing theory for advanced grid stiffened structures. Compos Part A Appl Sci Manuf 2002;33:155–61.
[12] Kim TD. Fabrication and testing of composite isogrid stiffened cylinder. Compos Struct 1999;45(1):1–6.
[13] Han DY, Tsai SW. Interlocked composite grids design and manufacturing. J Compos Mater 2003;37(4):287–316.
[14] Vasilliev VV, Barynin VA, Rasin AF. Anisogrid lattice structures – survey of development and application. Compos Struct 2001;54(2–3):361–70.
[15] Olsson KA. Sandwich structures for naval ships: design and experience. Mechanics of sandwich structures, ASME international mechanical engineering congress and exposition 2000.
[16] Li JH, Hunt JF, Cai ZY, Zhou XY. Bending analyses for 3D engineered structural panels made from laminated paper and carbon fabric. Compos Part B 2013;53:17–24.
[17] Li JH, Hunt JF, Gong SQ, Cai ZY. High strength wood-based sandwich panels reinforced with fiberglass and foam. Bioresources 2014;9(2):1898–913.
[18] Fang DL, Zhang YH, Chui XD. Mechanical properties and optimal design of lattice structures. Science Press; 2009.
[19] Ferreira AJM. Analysis of composite plates using a layerwise theory and multiquadrics discretization. Mech Adv Mater Struct 2005;12:99–112.
[20] Ferreira AJM, Roque CMC, Jorge RMN, Kansa EJ. Static deformations and vibration analysis of composite and sandwich plates using a layerwise theory and multiquadrics discretizations. Eng Anal Boundary Elem 2005;29:1104–14.
[21] Ferreira AJM, Roque CMC, Martins P. Analysis of composite plates using higher-order shear deformation theory and a finite point formulation based on the multiquadric radial basis function method. Compos B Eng 2003;34:627–36.
[22] Maturi DA, Ferreira AJM, Zenkour AM, Mashat DS. Analysis of sandwich plates with a new layerwise formulation. Compos B Eng 2014;56:484–9.
[23] Whitney JM. Structural analysis of laminated anisotropic plates. Lancaster, PA: Technomic Publishing Company Inc.; 1987.
[24] Chen Z, Wang BG. Elastic equivalent model of complex fiber reinforced plastic pavement deck. J Chang'an Univ 2007;27(5):24–9.
[25] Troitsky MS. Stiffened plate: bending, stability and vibrations. Amsterdam, NY: Elsevier Scientific Pub. Co; 1976.
[26] Li JH, Hunt JF, Gong SQ, Cai ZY, Wood-based tri-axial sandwich composite materials: design, fabrication, testing, modeling and application. In: CAMX Conference Proceedings, Orlando, FL, October 13–16; 2014. p. 232–247.
[27] Li JH, Hunt JF, Gong SQ, Cai ZY. Testing and evaluation of a slot and tab construction technique for light-weight wood-based structural panels under bending. J Test Eval 2016;40(1):1–10.
[28] Sun XF, Fang XS, Guan LT. Material mechanics. Beijing: Higher Education Publishing House; 2002.
[29] ASTM D638-2010. Standard test method for tensile properties of plastics. ASTM Standards International.
[30] ASTM D695-2010. Standard test method for compressive properties of rigid plastics. ASTM Standards International.
[31] ASTM C393-2006. Standard test method for core shear properties of sandwich constructions by beam. ASTM Standards International.
[32] ASTM D5868-01. Standard Test Method For Lap Shear Adhesion For Fiber Reinforced Plastic (FRP) bonding. ASTM Standards International.